*Progress In Electromagnetics Research, PIER 30, 191–211, 2001*

# REFLECTION AND TRANSMISSION OF X-WAVES IN THE PRESENCE OF PLANARLY LAYERED MEDIA: THE PULSED PLANE WAVE REPRESENTATION

A. M. Attiya and E. El-Diwany

Department of Microwave Engineering
Electronic Research Institute, Dokki
Giza, 12211, Egypt

A. M. Shaarawi

Department of Engineering Physics and Mathematics
Faculty of Engineering, Cairo University
Giza 12211, Egypt

I. M. Besieris

The Bradley Department of Electrical and Computer Engineering
Virginia Polytechnic Institute and State University
Blacksburg, Virginia 24061, USA

**Abstract**–In this paper, a general ray-theoretical representation of the X-wave pulse is introduced. This representation is based on pulsed plane waves having wave vectors lying on a conic surface. The pulsed plane wave representation is used to study the behavior of X-waves in the presence of planarly layered media. In the case of an interface separating two semi-infinite media, the pulsed plane wave representation provides a clear explanation for the disintegration of the transmitted field. It shows that unlike the incident and reflected fields, the wave vectors associated with the transmitted field do not lie on a cone. Furthermore, this approach allows one to estimate several characteristic properties of the layered media (e.g., dielectric constant and thickness of each layer) from the time of arrival of the reflected X-waves.

## 1. INTRODUCTION

In 1983 Brittingham introduced a new solution to the three-dimensional time-dependent Maxwell equations in the form of a packet-like, nondispersive wave; namely, the Focus Wave Mode (FWM) [1]. This solution represents a localized wave field concentrated in a three-dimensional moving volume. Brittingham's pioneering work was an introduction to a large number of slowly decaying wave solutions such as the scalar FWM [2, 3], the Modified Power Spectrum pulse [4], Electromagnetic Missiles [5, 6], Pulsed Beams [7, 8], Pulsed Bessel Beams [9, 10] and X-waves [11, 12]. All these solutions share a common feature; namely, that they represent three-dimensional localized wave packets undergoing very slow dispersion over an extended focus depth. These properties make them good candidates for many applications involving detection and identification of scattering objects, e.g., ground penetrating radar [13] and impulse radar [14]. Other possible applications include secure communications and remote sensing.

It has been pointed out recently that two of the aforementioned solutions exhibit similar spectral structures [15, 16]. Specifically, it has been shown that FWMs and X-waves have a characteristic spectral coupling between their temporal and spatial frequency variables. Such coupling is responsible for the unusual spatio-temporal properties of these two classes of solutions and is accountable for their slow decay properties [16, 17]. Therefore, X-wave and FWM-type solutions may be perceived as two distinct branches of a single more general class of wave solutions; namely, localized waves (LW). An analysis of the properties of an X-wave based on its angular spectrum has established that its wave vectors lie on a conic surface whose apex angle is a parameter appearing explicitly in the X-wave solution [18, 19]. In contradistinction, an angular spectrum representation of the FWM field reveals that its wave vectors form a weighted distribution over an infinite number of uniaxial cones [20]. The apex angles can take any values between

0 to $\pi$; consequently, components traveling in opposite directions contribute to the total field. For situations involving layered media, it is preferable to deal with fields traveling only in one direction. For this reason, our analysis in the rest of this paper will be based on the X-wave.

The reflection and transmission of LWs from an interface separating two different materials has been discussed in two earlier papers [21, 22]. In both cases, the authors used a two-dimensional variation of Brittingham's FWM solution. Both papers agree on the fact that for normal incidence the reflected and transmitted fields preserve their LW structure. They have also shown that the transmitted field does not have a LW structure. In this work, we use a ray-theoretic approach based on a general pulsed plane wave representation to explain how the transmitted field loses its LW character. Unlike previous work, the analysis adopted in this paper deals with three-dimensional LWs of the X-wave type. The ideas introduced in this paper provide a clear mental picture of the reflection and transmission processes within a ray-theoretic framework. This is crucial in any analysis dealing with inhomogeneities or multi-layered media. The general ray-theoretic approach advocated in this paper is complemented in an accompanying paper [23]. The latter provides a comprehensive spectral analysis of the reflection and transmission of a three-dimensional electromagnetic X-wave obliquely incident on an air-dielectric interface. Another relevant work deals with the reflection and transmission of an acoustic X-wave incident on a planar interface separating two media [24]. In these two articles the Fourier representation of the incident, reflected and transmitted fields are transformed into an azimuthal angular representation. This angular superposition, closely related to the pulsed plane wave representation described in this paper, is used to calculate the amplitudes of the reflected and transmitted fields for both the electromagnetic and acoustic X-waves.

The plan of this work is to provide a general pulsed plane wave representation of X wave-type fields and to use such a representation within a ray-theoretic framework to study the behavior of reflected and transmitted X-waves. In Sec. 2, it is shown that the X wave-type solutions can be represented as angular superpositions of analytic signals [cf. Eq. (11)]. These analytic signals depict the transient character of the pulses considered. Building on such a representation, it is shown that an X-wave pulse corresponds to a superposition over plane waves

having wave vectors lying on a circular cone, with each plane wave component time-limited by a Lorentzian window. Subsequently, this representation is extended into a ray-theoretic framework which provides a simple mental picture of the behavior of X-waves. In Sec. 3, we study the reflection and transmission of an X-wave pulse incident on a planar interface. We use the fact that the incident X-wave field components have wave vectors defined on a single cone to demonstrate that the wave vectors associated with the reflected plane wave components are also defined on a single cone. As a consequence, the reflected field preserves its LW structure. It is then shown that the transmitted field components have wave vectors lying on a convoluted conic surface. This surface results from deforming a regular cone by stretching its apex into a line segment; the latter acquires larger lengths as the transmitted pulse moves away from the interface. This effect causes the transmitted field to disperse with distance. Our ray-theoretic approach reveals that the deformation of the conic surface results from either an outward or an inward elongation of the apex point into a line segment depending on whether $(c_1/c_2) > 1$ or $(c_1/c_2) < 1$, where $c_1$ and $c_2$ denote propagation speeds in the two media. In Sec. 4, we demonstrate that for multi-layered media, X-waves can be used to deduce the dielectric constant and the thickness of the various layers as an inverse problem.

## 2. THE PULSED PLANE WAVE REPRESENTATION OF X-WAVES

To study the reflection and transmission of X-waves from a planar surface of discontinuity, it is advantageous to represent them as a superposition of pulsed plane waves having wave vectors lying on a circular conic surface. In this section, we introduce two useful representations. The first is a general pulsed plane wave superposition that will be used in later sections. The second is a generalization of the azimuthal angular superposition introduced previously in Ref. 24 for acoustic X-waves. The same representation is used in Ref. 23 to calculate the amplitudes of the reflected and transmitted electromagnetic X-waves.

We start with the Weyl representation of unidirectional (along the positive $z$-direction) solutions of the homogeneous wave equation in free space; specifically,

$$\psi(x, y, z, t) = \mathrm{Re}(\Psi(x, y, z, t)) \tag{1a}$$

where

$$\Psi(x,y,z,t) = \frac{1}{\pi}\int_0^{\infty} d\omega \int_{-\infty}^{+\infty} dk_x \int_{-\infty}^{+\infty} dk_y e^{i\omega t} e^{-ik_x x} e^{-ik_y y} \cdot e^{-iz\sqrt{(\omega/c)^2-\left(k_x^2+k_y^2\right)}} \Phi(k_x,k_y,\omega). \tag{1b}$$

We introduce, next, a change of the transverse wave numbers as follows:

$$k_x = \chi\cos\phi, \quad k_y = \chi\sin\phi \quad \text{and} \quad \chi \equiv \sqrt{k_x^2+k_y^2}. \tag{2}$$

With this change of variables, Eq. (1b) becomes

$$\Psi(x,y,z,t) = \frac{1}{\pi}\int_0^{\infty} d\omega \int_0^{2\pi} d\phi \int_0^{\infty} d\chi\chi e^{i\omega t} e^{-i\chi(x\cos\phi+y\sin\phi)} \cdot e^{-iz\sqrt{(\omega/c)^2-\chi^2}} \widetilde{\Phi}(\chi,\phi,\omega). \tag{3}$$

For an X-wave type solution, we specify the spectrum:

$$\widetilde{\Phi}(\chi,\phi,\omega) = (1/\chi)\delta\left(\chi-(\omega/c)\sin\xi\right)\Phi_0(\phi,\omega). \tag{4}$$

Using it in conjunction with Eq. (3), we obtain

$$\Psi(x,y,z,t) = \frac{1}{\pi}\int_0^{2\pi} d\phi \int_0^{\infty} d\omega e^{i\omega t} e^{-i(\omega/c)\sin\xi(x\cos\phi+y\sin\phi)} \cdot e^{-iz(\omega/c)\cos\xi}\Phi_0(\phi,\omega). \tag{5}$$

The axicon angle $\xi$ is defined over the range $0 < \xi < \pi/2$. The transverse spectral variable $\chi$ in Eq. (4) assumes positive values and $\cos\xi > 0$. As a consequence, Eq. (5) can be rewritten as

$$\Psi(x,y,\tau) = \frac{1}{\pi}\int_0^{2\pi} d\phi \int_0^{\infty} d\omega e^{i\omega[\tau-(\sin\xi/c)(x\cos\phi+y\sin\phi)]}\Phi_0(\phi,\omega), \tag{6}$$

where $\tau = t-(z/v)$ and $v = (c/\cos\xi)$ being a superluminal speed, i.e., $v > c$. By virtue of the principle of linear superposition,

$$\Psi_e(x,y,z,\tau) = e^{i\omega[\tau-(\sin\xi/c)(x\cos\phi+y\sin\phi)]} \tag{7}$$

is an elementary solution to the homogeneous scalar wave equation. It represents a plane wave moving along the direction of the wave vector

$$\vec{k} = (\omega/c)\sin\xi\cos\phi\vec{u}_x + (\omega/c)\sin\xi\sin\phi\vec{u}_y + (\omega/v)\vec{u}_z. \qquad (8)$$

The family of all vectors defined by Eq. (8) lie on the surface of a circular cone having an apex angle $\xi$. Note that the phase speed along the direction of propagation of each plane wave is given by $\omega/\left|\vec{k}\right| = c$. The speed along the positive $z$-direction is equal to $v > c$, which is a fundamental property of all X wave-type solutions. It is thus clear that as $\phi$ takes on values from 0 to $2\pi$, the angular superposition given in Eq. (6) consists of plane waves with wave vectors $\vec{k}$ lying on the surface of a circular cone with an apex angle equal to $\xi$. Such a conic surface is shown in Fig. 1.

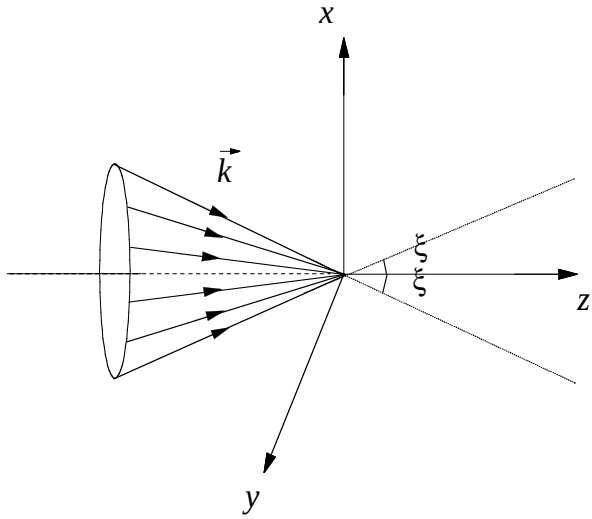


**Figure 1.** The conic surface formed by the wave vectors associated with the plane wave components of an X-wave traveling in the positive $z$ direction.

If the spectrum $\Phi_0(\phi,\omega)$ has a broad bandwidth, the field $\Psi(x,y,\tau)$ can be perceived as a superposition over pulsed plane waves having $\vec{k}$ vectors lying on the aforementioned conic surface. Considering the pulsed plane wave representation given in Eq. (6), we assume that the spectrum $\Phi_0(\phi,\omega)$ is separable, viz.,

$$\Phi_0(\phi,\omega) = f(\phi)G(\omega). \qquad (9)$$

Furthermore, we let $g^+(t)$ denote the complex analytic signal corresponding to the temporal spectrum $G(\omega)$, namely,

$$g^+(t) = \frac{1}{\pi}\int_0^\infty d\omega e^{i\omega t} G(\omega), \qquad \mathrm{Im}(t) > 0. \tag{10}$$

Under these conditions, the X wave-type solution $\Psi(x, y, \tau)$ of the homogeneous scalar wave equation can be written as follows:

$$\Psi(x, y, \tau) = \int_0^{2\pi} d\phi F(\phi) g^+ \left[\tau - (\sin\xi/c)(x\cos\phi + y\sin\phi)\right]. \tag{11}$$

It is seen, then, that the wave function $\Psi(x, y, \tau)$ is expressed as an angular superposition of pulsed waves. The azimuthal angular superposition deduced in Ref. 24 through a transformation of variables of the Fourier representation of the obliquely incident, reflected and transmitted scalar X-waves is a special case of this more general representation. This formulation provides the possibility of obtaining a large class of interesting X-wave-type localized solutions. Of course, each solution in this class is characterized by an infinite energy content because it propagates superluminally along the positive $z$-direction without any distortion.

The zero-order X-wave follows from Eq. (11) by choosing $F(\phi) = 1$ and $G(\omega) = e^{-(\omega/c)a}$, $a > 0$. In this case,

$$g^+(t) = \frac{1}{\pi}\int_0^\infty d\omega e^{i\omega t} e^{-(\omega/c)a} = \frac{1}{\pi}\int_0^\infty d\omega e^{-(\omega/c)(a-ict)} = \frac{1}{\pi}\frac{c}{(a-ict)}. \tag{12}$$

This represents a Lorentzian time window applied to the plane wave components associated with the various wave vectors lying on the circular cone shown in Fig. 1. Substituting Eq. (12) in the superposition given in Eq. (11), we obtain

$$\begin{aligned}\Psi_{XW}(x, y, \tau) &= \frac{c}{\pi}\int_0^{2\pi} d\phi \frac{1}{a - ic\left[\tau - \sin\xi/c(x\cos\phi + y\sin\phi)\right]} \\ &= \frac{c}{\pi}\int_0^{2\pi} d\phi \frac{1}{a + i(z\cos\xi - ct) + i\sin\xi(x\cos\phi + y\sin\phi)}.\end{aligned} \tag{13}$$

This is a special angular superposition of pulsed waves. Its form is reminiscent of that for the incident field ($\alpha_1 = 0$) given in Eq. (30)

in Ref. 24. The two representations can be related through a simple change of variables. The integration over $\phi$ can be carried out using formula (3.661.4) in Ref. 25 to give

$$\Psi(\vec{r},t) = \frac{c}{\left[\rho^2 \sin^2\xi + (a + i(z\cos\xi - ct))^2\right]^{1/2}}. \tag{14}$$

Notice that other choices of the spectrum $G(\omega)$ result in different X wave-type solutions. For example, the choice $G(\omega) = \sqrt{\omega/\omega_0}\exp\left\{-T^2(\omega-\omega_0)^2\right\}$ yields the Bessel X-pulse [10]. For short values of $T \sim (2\pi/\omega_0)$, we get an X-shaped field with a Gaussian temporal profile near the peak of the pulse. Thus, it has been shown that the general representation given in Eq. (11) covers a large class of pulsed fields. In the subsequent sections we use a ray-theoretic framework that emulates the angular superposition over pulsed waves [cf. Eq. (6)] to study the reflection and transmission properties of X wave-type solutions. The azimuthal angular representation given in Eq. (11) is used in Ref. 23 to calculate the reflected and transmitted fields due to an electromagnetic X-wave incident on a surface of discontinuity.

The pulsed plane wave components of the X wave-type fields can be represented graphically by the pulsed waves traveling along the wave vectors lying on a circular cone. This is shown schematically in Fig. 2 were only two rays are shown in a horizontal section of the conic surface. The two associated pulsed fields are sketched at different times $t_1$ and $t_2$. The heavy line in the middle represents the peak of the pulsed plane wave, while the two lighter lines specify its temporal width. The localized part of the field occurs at the intersection of the two pulsed plane waves. From this graphical representation, it is straightforward to see that the pulsed plane waves move along the conic surface with velocity $c$. The intersection point of the pulsed plane waves, corresponding to the peak of the X-wave, moves at velocity $v = c/\cos\xi$. Additional information can be deduced from schematics of this type. In Fig. 3, the pulsed-widths of the plane wave components are enlarged to demonstrate how one can obtain estimates of the lateral width (waist) and the axial width of the X-wave field. It is shown here that pulsed plane wave components having widths equal to $a$ result in an X-wave having lateral and axial waists equal to $a/\sin\xi$ and $a/\cos\xi$, respectively. These values agree with previous estimates [12, 16, 26] deduced from the explicit form of the X-wave solution given in Eq. (14). One should also notice that the maximum of the temporal frequency

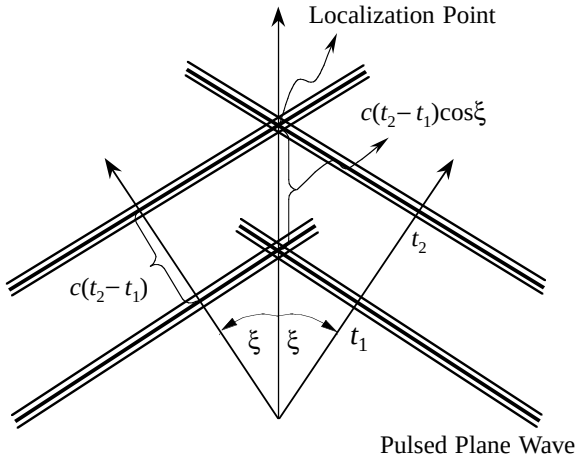


**Figure 2.** Schematic representation of the pulsed wave components traveling along the conic surface. The peak of the X-wave is formed at the intersection point.

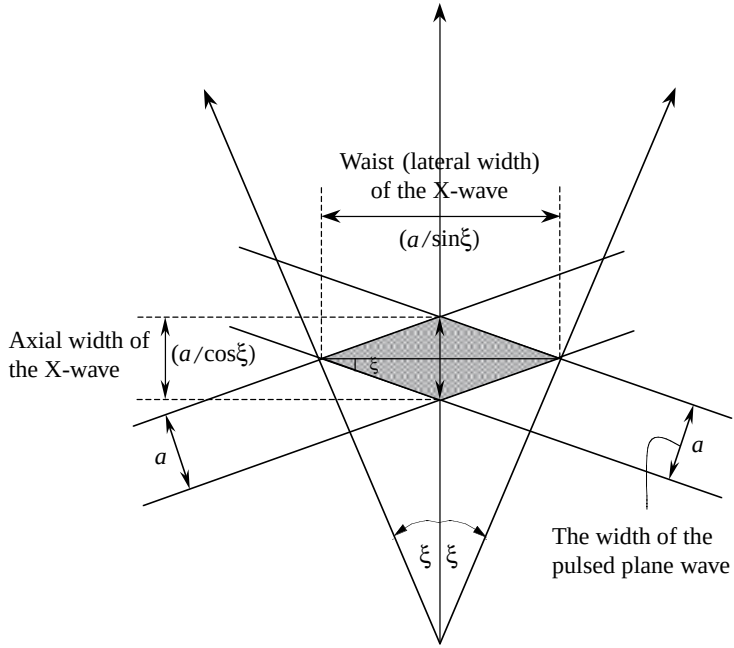


**Figure 3.** The axial and lateral widths of the X-wave and their relation to the width of the pulsed plane wave components.

of the X-wave is equal to that of the pulsed plane wave components. In particular, $\omega_{\max} = 4c/a$ corresponding to the point at which the temporal spectrum decays to $1/e^4$ of the peak value of the spectrum [16].

## 3. BEHAVIOR OF AN X-WAVE INCIDENT ON A PLANAR INTERFACE

In this section, the pulsed plane wave representation is used to study the behavior of an X-wave incident on a planar interface separating two electrically different media. We start by considering the simple case of an X-wave normally incident on an air-dielectric interface. In this situation, all the pulsed plane wave components are symmetrically tilted at angle $\xi_0$ with respect to the normal to the interface. The reflected wave vectors form a cone having the same apex angle $\xi_0$ as is the case for the incident field. According to Snell's law, the incident plane wave components are transmitted with an angle $\xi_1 = \sin^{-1}\left(\sin\xi_0/\sqrt{\varepsilon_1}\right)$, where the first medium is air and the second one is a dielectric having relative permittivity $\varepsilon_1$. It should be noted that for an X-wave, the reflection and transmission coefficients of each tilted plane wave component are not frequency dependent [23, 24]. Furthermore, for normal incidence the reflection and transmission coefficients are independent of the azimuthal variable $\phi$. This is not the case when an X-wave is obliquely incident on the surface of discontinuity. In this situation, the reflection and transmission coefficients of the plane wave components depend on $\phi$ [23]. Thus, for normal incidence, the reflection and transmission coefficients can be treated as numerical factors multiplying the reflected and transmitted field components. As a consequence, the wave vectors of the reflected and transmitted components lie on conic surfaces. This causes the reflected and transmitted pulses to preserve their LW structure.

The schematic diagram shown in Fig. 4 illustrates that the incident and reflected cones have the same apex angle $\xi_0$. The transmitted cone on the other hand has an apex angle equal to $\xi_1$. The velocity of the peak of the transmitted X-wave can also be deduced [cf. Fig. 2] to obtain

$$v_1 = (c_1/\cos\xi_1) = c/\left(\sqrt{\varepsilon_1}\cos\left(\sin^{-1}\left(\sin\xi_0/\sqrt{\varepsilon_1}\right)\right)\right), \qquad (15)$$

where $c$ is the wave speed in air. This means that the ratio $v_1/v_0$ is less than $1/\sqrt{\varepsilon_1}$ by a factor equal to $\cos\xi_0/\cos\xi_1$. Here, $v_0 =$

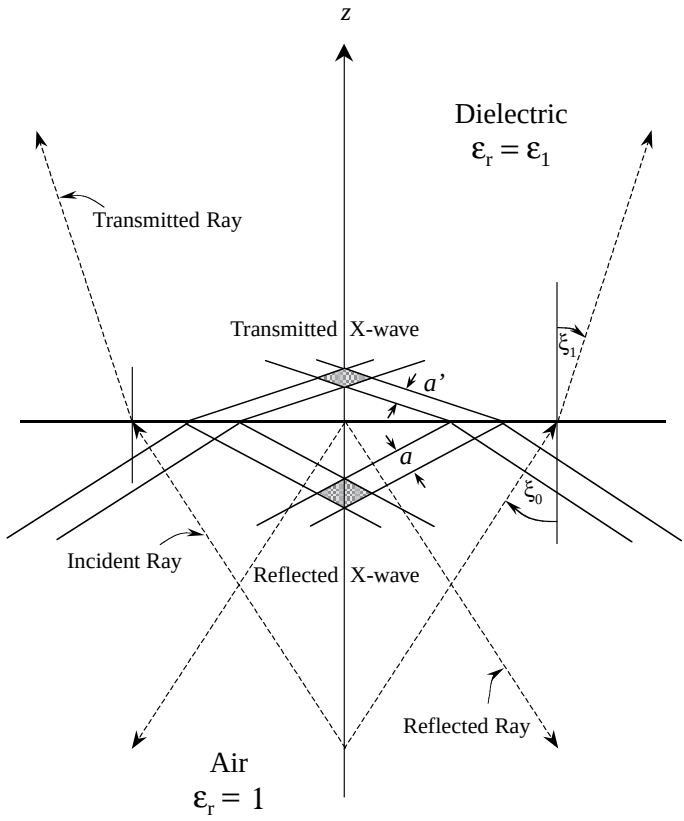


**Figure 4.** Schematic representation of the pulsed plane wave representation of the reflected and transmitted X-waves together with the associated conic rays.

$c/\cos\xi_0$ is the speed of the peak of the X-wave in air. The schematic diagram in Fig. 4 provides a clear mental picture of several fundamental properties of the reflected and transmitted fields. In particular, it can be seen that the lateral and axial widths of the reflected X-wave are the same as those of the incident field. For the transmitted X-wave, the width of the transmitted pulsed plane wave components changes to $a' = a(\sin\xi_1/\sin\xi_0) = a/\sqrt{\varepsilon_1}$. The lateral waist of the transmitted field is unchanged since it equals $(a'/\sin\xi_1) = (a/\sin\xi_0)$. The transmitted field X-wave, however, is compressed along the direction of propagation, where the axial-width of the transmitted pulse equals $a'/\cos\xi_1 = a/\left(\sqrt{\varepsilon_1}\cos\xi_1\right)$. This compression of the transmitted X-

wave can cause the peak amplitude of the transmitted field to be larger than that of the incident X-wave.

For an obliquely incident X-wave, the situation is slightly more involved. In this case, the circular conic surface comprising the wave vectors associated with the different plane wave components is rotated as shown in Fig. 5. The X-wave is assumed incident from the negative $z$ direction on a planar interface situated at $z = -d_0$. The obliquely incident X-wave is obtained by rotating its wave vectors through an angle $\alpha$ around the $x$-axis as shown in Fig. 5. This situation is equivalent to rotating the $yz$ plane by an angle $\alpha$. The original coordinates can be expressed in terms of the rotated ones as follows:

$$\begin{aligned} x &= x' \\ y &= y'\cos\alpha - z'\sin\alpha, \\ z &= y'\sin\alpha - z'\cos\alpha. \end{aligned} \tag{16}$$

Combining these rotational transformations with the following coordinate relationships

$$x = r\sin\theta\cos\phi \qquad y = r\sin\theta\sin\phi \qquad z = r\cos\theta, \tag{17a}$$

$$x' = r\sin\theta'\cos\phi' \qquad y' = r\sin\theta'\sin\phi' \qquad z' = r\cos\theta', \tag{17b}$$

we can relate the angles $(\theta, \phi)$ associated with each incident wave vector to the rotated angular variables $(\theta', \phi')$; specifically,

$$\theta(\theta', \phi') = \cos^{-1}(\sin\theta'\sin\alpha\sin\phi' + \cos\theta'\cos\alpha), \tag{18a}$$

$$\begin{aligned} \phi(\theta', \phi') = \cos^{-1}\big(&\sin\theta'\cos\phi'/\sin\big(\cos^{-1} \\ &\cdot(\sin\theta'\sin\alpha\sin\phi' + \cos\theta'\cos\alpha)\big)\big), \text{ or} \end{aligned} \tag{18b}$$

$$\begin{aligned} \phi(\theta', \phi') = \sin^{-1}\big(&(\sin\theta'\cos\alpha\sin\phi' - \cos\theta'\sin\alpha)/\sin\big(\cos^{-1} \\ &\cdot(\sin\theta'\sin\alpha\sin\phi' + \cos\theta'\cos\alpha)\big)\big). \end{aligned} \tag{18c}$$

To determine the points of intersection of the wave vectors of the incident X-wave, we set $z = -d_0$ at the planar interface. The radial distances defining the various points lying on the planar interface are $r = -d_0/\cos\theta$. The position vector $\vec{r}$ defining the different points on the surface of discontinuity has $\pi \geq \theta > (\pi/2)$. Consequently, the $x$ and $y$ coordinates of these points can be written as

$$x(\theta', \phi') = -d_0\frac{\sin\theta'\cos\phi'}{\sin\theta'\sin\alpha\sin\phi' + \cos\theta'\cos\alpha}, \tag{19a}$$

$$y(\theta', \phi') = -d_0\frac{\sin\theta'\cos\alpha\sin\phi' - \cos\theta'\sin\alpha}{\sin\theta'\sin\alpha\sin\phi' + \cos\theta'\cos\alpha}. \tag{19b}$$

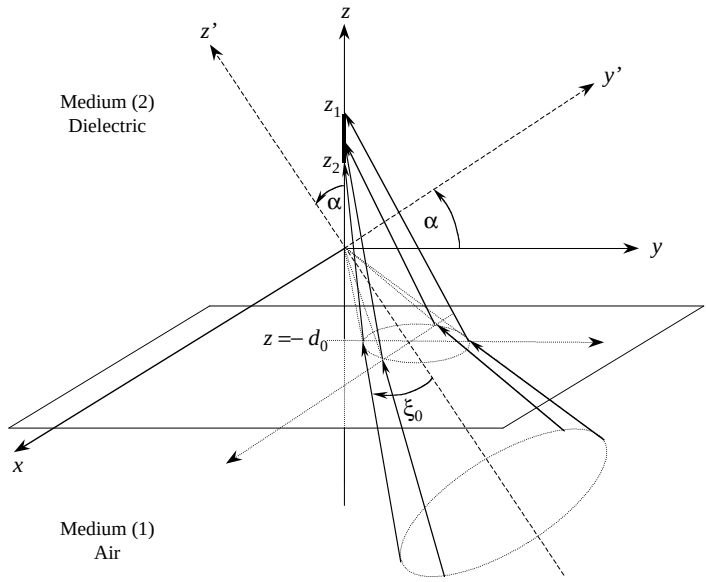


(a)

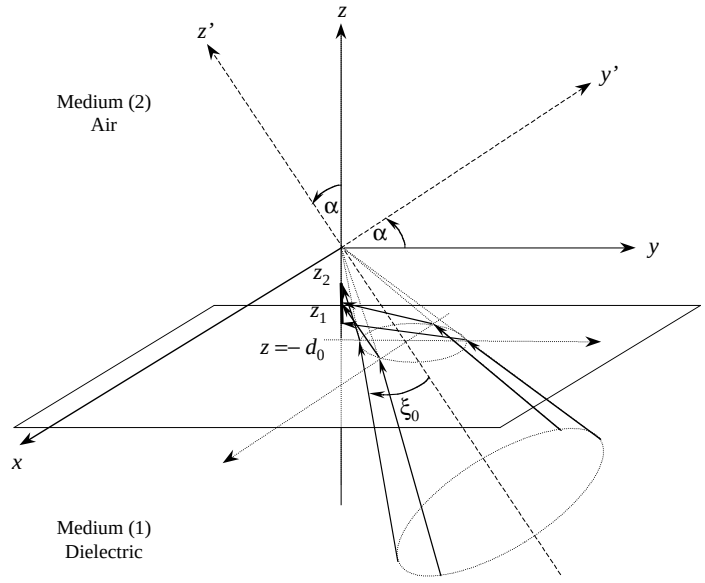


(b)

**Figure 5.** Geometrical ray representation of an obliquely incident X-wave on an interface situated at $z = -d_0$ for: (a) $(c_1/c_2) > 1$ and (b) $(c_1/c_2) < 1$ .

At the points of intersection of the wave vectors with the surface of discontinuity, the spectral angular variable $\theta_k$ associated with each $\vec{k}$ vector is related to the variable $\theta$ defining the position vector $\vec{r}$ through the relation $\theta = \pi - \theta_k$. The wave vectors associated with the pulsed plane wave components of the obliquely incident X-wave have $\theta'_k = \xi_0$. This results in a rotated position angular variable $\theta' = \pi - \xi_0$. The angular directions of the incident rays, thus, become

$$\theta_0(\phi') = \cos^{-1}(\sin\xi_0 \sin\alpha \sin\phi' - \cos\xi_0 \cos\alpha), \tag{20a}$$

$$\phi_0(\phi') = \cos^{-1}\left(\sin\xi_0 \cos\phi' / \sin \cdot \left(\cos^{-1}(\sin\xi_0 \sin\alpha \sin\phi' - \cos\xi_0 \cos\alpha)\right)\right), \text{ or} \tag{20b}$$

$$\phi_0(\theta') = \sin^{-1}\left((\sin\xi_0 \cos\alpha \sin\phi' + \cos\xi_0 \sin\alpha)/\sin \cdot \left(\cos^{-1}(\sin\xi_0 \sin\alpha \sin\phi' - \cos\xi_0 \cos\alpha)\right)\right). \tag{20c}$$

The substitution of the value $\theta' = \pi - \xi_0$ in Eq. (19) gives the locations of the points of intersection of the various rays with the planar interface; specifically,

$$x_0 = -d_0 \frac{\sin\xi_0 \cos\phi'}{\sin\xi_0 \sin\alpha \sin\phi' - \cos\xi_0 \cos\alpha}, \tag{21a}$$

$$y_0 = -d_0 \frac{\sin\xi_0 \cos\alpha \sin\phi' + \cos\xi_0 \sin\alpha}{\sin\xi_0 \sin\alpha \sin\phi' - \cos\xi_0 \cos\alpha}. \tag{21b}$$

In free space, the wave vectors of the X-wave intersect at the origin as illustrated by the dotted rays in Fig. 5. Because the two media are different, the transmitted rays will refract according to the following equations:

$$x - x_0 = (z - z_0)\tan\theta_1 \cos\phi_1, \tag{22a}$$

$$y - y_0 = (z - z_0)\tan\theta_1 \sin\phi_1. \tag{22b}$$

Here, $(\theta_1,\ \phi_1)$ are the angular directions defining the transmitted wave vectors. If the dielectric constant of the material under the interface is $\varepsilon_1$, the angular directions of the transmitted rays in the second medium are given by

$$\sin\theta_1 = \sin\theta_0/\sqrt{\varepsilon_1} = \sin\left(\cos^{-1}(\sin\xi_0 \sin\alpha \sin\phi' \cos\xi_0 \cos\alpha)\right)/\sqrt{\varepsilon_1}, \tag{23a}$$

$$\begin{aligned}\cos\phi_1 &= \cos\phi_0 \\ &= \sin\xi_0\cos\phi'/\sin\left(\cos^{-1}(\sin\xi_0\sin\alpha\sin\phi' - cos\xi_0\cos\alpha)\right), \quad (23b)\\ \sin\phi_1 &= \sin\phi_0 \\ &= (\sin\xi_0\cos\alpha\sin\phi' + \cos\xi_0\sin\alpha)/\sin \\ &\quad \cdot\left(\cos^{-1}(\sin\xi_0\sin\alpha\sin\phi' - \cos\xi_0\cos\alpha)\right). \quad (23c)\end{aligned}$$

By combining Eqs. (21–23), we deduce the following equations of the transmitted rays:

$$x = x_0 + (z - z_0)\frac{\sin\xi_0\cos\phi'}{\sqrt{\varepsilon_1 - 1 + (\sin\xi_0\sin\alpha\sin\phi' - \cos\xi_0\cos\alpha)^2}}, \quad (24a)$$

$$y = y_0 + (z - z_0)\frac{\sin\xi_0\cos\alpha\sin\phi' + \cos\xi_0\sin\alpha}{\sqrt{\varepsilon_1 - 1 + (\sin\xi_0\sin\alpha\sin\phi' - \cos\xi_0\cos\alpha)^2}}. \quad (24b)$$

Any two rays identified by the angular directions $\phi' = (\pi/2) - \phi_0$ and $\phi' = (\pi/2) + \phi_0$ are symmetric with respect to the $yz$ plane and their coordinates are given as follows:

$$\begin{aligned}&x\left((\pi/2) - \phi_0\right) = -x\left((\pi/2) + \phi_0\right) \\ &= -d_0\frac{\sin\xi_0\sin\phi_0}{\sin\xi_0\sin\alpha\cos\phi_0 - \cos\xi_0\cos\alpha} \\ &\quad + (z + d_0)\frac{\sin\xi_0\sin\phi_0}{\sqrt{\varepsilon_1 - 1 + (\sin\xi_0\sin\alpha\cos\phi_0 - \cos\xi_0\cos\alpha)^2}}, \quad (25a)\\ &y\left((\pi/2) - \phi_0\right) = y\left((\pi/2) + \phi_0\right) \\ &= -d_0\frac{\sin\xi_0\cos\alpha\cos\phi_0 + \cos\xi_0\sin\alpha}{\sin\xi_0\sin\alpha\cos\phi_0 - \cos\xi_0\cos\alpha} \\ &\quad + (z + d_0)\frac{\sin\xi_0\cos\alpha\cos\phi_0 + \cos\xi_0\sin\alpha}{\sqrt{\varepsilon_1 - 1 + (\sin\xi_0\sin\alpha\cos\phi_0 - \cos\xi_0\cos\alpha)^2}}. \quad (25b)\end{aligned}$$

The two rays corresponding to $\phi' = (\pi/2) - \phi_0$ and $\phi' = (\pi/2) + \phi_0$ intersect at the following coordinates:

$$\begin{aligned}&x\left((\pi/2) - \phi_0\right) = x\left((\pi/2) + \phi_0\right) = 0, \quad (26a)\\ &y\left((\pi/2) - \phi_0\right) = y\left((\pi/2) + \phi_0\right) = 0, \quad (26b)\\ &z\left((\pi/2) - \phi_0\right) = z\left((\pi/2) + \phi_0\right) \\ &\quad = d_0\left\{\sqrt{1 + (\varepsilon_1 - 1)/(\sin\xi_0\sin\alpha\cos\phi_0 - \cos\xi_0\cos\alpha)^2} - 1\right\}. \quad (26c)\end{aligned}$$

This means that each pair of symmetric rays intersects on the $z$-axis. However, the point of intersection on the $z$-axis depends on the azimuthal angle $\phi_0$. Thus, the wave vectors of the transmitted pulse do not lie on a circular cone. Instead, they form a convoluted conic surface for which the apex point has been stretched into a line segment. The two end points of such a line segment correspond to $\phi_0 = 0$ and $\phi_0 = \pi$. Specifically,

$$z_1 = z(\pi/2) = d_0 \left\{ \sqrt{1 + (\varepsilon_1 - 1)/\cos^2(\alpha + \xi_0)} - 1 \right\} \tag{27a}$$

$$z_2 = z(-\pi/2) = d_0 \left\{ \sqrt{1 + (\varepsilon_1 - 1)/\cos^2(\alpha - \xi_0)} - 1 \right\}. \tag{27b}$$

The difference between these two values, viz.,

$$\Delta z = d_0 \left\{ \sqrt{1 + (\varepsilon_1 - 1)/\cos^2(\alpha + \xi_0)} - \sqrt{1 + (\varepsilon_1 - 1)/\cos^2(\alpha - \xi_0)} \right\}, \tag{28}$$

is the length of the aforementioned line segment. Its length increases with the distance $d_0$ away from the interface. This increase in the length of the line segment is responsible for the dispersion of the spectral components of the transmitted field and causes the pulse to decay with distance.

According to Eqs. (26) and (27), an X-wave incident from the side of the air layer $(\varepsilon_1 > 1)$ produces a transmitted field characterized by a convoluted conic surface whose line segment is stretched outwards with $z_1 > z_2$. For an X-wave incident from the dielectric layer, the relative permittivity $\varepsilon_1$ in Eqs. (26) and (27) has to be replaced by $(1/\varepsilon_1) < 1$. In this case, the line segment associated with the convoluted conic surface is pulled inwards toward the interface resulting in having $z_2 > z_1$. Pulsed plane wave components incident at angles greater than the critical angle have complex $z_1$ values with the real part equal to $-d_0$. This corresponds to having evanescent wave components moving laterally on the interface. A detailed spectral analysis of these waves is provided in Ref. 24 for the case of acoustic scalar X-waves.

## 4. X-WAVE NORMALLY INCIDENT ON PLANARLY MULTI-LAYERED MEDIA

In the case of a multi-layered structure below the upper air-dielectric interface, the transmitted X-wave is multiply reflected inside each layer and the reflected X-wave is retransmitted into free space. For a certain

observation point at a height $d_0$ above the air-dielectric interface, the incident pulse is observed first. Then, the reflected pulse from the air-dielectric interface is observed after a time $t_1 = 2d_0/(c/\cos\xi_0)$. The first reflected pulse from the second interface is observed after a time $t_2 = 2d_0/(c/\cos\xi_0) + 2d_1/(c_1/\cos\xi_1)$, where $d_1$ is the thickness of the first layer. Henceforth, multiple reflections are observed. By measuring $t_1$ and $t_2$ for two different X-waves with different $\xi_0$ angles, one obtains the following two simultaneous transcendental equations in two unknowns, namely, the thickness $d_1$ and the dielectric constant $\varepsilon_1$:

$$\Delta t^{(1)} = t_2^{(1)} - t_1^{(1)} = 2d_1 / \left\{ c/\sqrt{\varepsilon_1} \cos\left( \sin^{-1}\left( \xi_0^{(1)} / \sqrt{\varepsilon_1} \right) \right) \right\}, \tag{28a}$$

$$\Delta t^{(2)} = t_2^{(2)} - t_1^{(2)} = 2d_1 / \left\{ c/\sqrt{\varepsilon_1} \cos\left( \sin^{-1}\left( \xi_0^{(2)} / \sqrt{\varepsilon_1} \right) \right) \right\}. \tag{28b}$$

Each of the two time differences $\Delta t^{(1)}$ and $\Delta t^{(2)}$ is satisfied by a different combination of $\varepsilon_1$ and $d_1$. We can obtain graphical solutions to Eqs. (28a,b) by plotting $\varepsilon_1$ vs. $d_1$ for different values of $\Delta t^{(1)}$ and $\Delta t^{(2)}$. Intersection points give the required values of $\varepsilon_1$ and $d_1$. The two equations in (28) can, however, be solved explicitly to yield

$$\varepsilon_1 = \frac{\sin^2 \xi_0^{(1)} - \left( \Delta t^{(1)} / \Delta t^{(2)} \right)^2 \sin^2 \xi_0^{(2)}}{1 - \left( \Delta t^{(1)} / \Delta t^{(2)} \right)^2}, \tag{29a}$$

$$d_1 = \frac{1}{2} \sqrt{\frac{\left( c\Delta t^{(1)} \right)^2 - \left( c\Delta t^{(2)} \right)^2}{\sin^2 \xi_0^{(2)} - \sin^2 \xi_0^{(1)}}}. \tag{29b}$$

These two expressions can be used to determine $\varepsilon_1$ and $d_1$. For example, consider using two X-waves having axicon angles $\xi_0^{(1)} = 20^\circ$ and $\xi_0^{(2)} = 40^\circ$ and that the two time intervals $\Delta t^{(1)} = 39.411\,\text{nsec}$ and $\Delta t^{(2)} = 37.878\,\text{nsec}$ have been measured. From the formulas given in Eqs. (29a,b), the dielectric constant of the first layer is $\varepsilon_1 = 4$ and its thickness is $d_1 = 3\,\text{m}$.

After determining $d_1$ and $\varepsilon_1$ for the first layer, the times of arrival of all reflections $m$ from the first layer can be calculated as

$$t_m^{(1)} = 2d_0 / \left\{ c/\cos\xi_0^{(1)} \right\} + 2md_1 / \left\{ c/\sqrt{\varepsilon_1} \cos\left( \sin^{-1}\left( \sin\xi_0^{(1)} / \sqrt{\varepsilon_1} \right) \right) \right\} \tag{30a}$$

$$t_m^{(2)} = 2d_0 / \left\{ c/\cos\xi_0^{(2)} \right\} + 2md_1 / \left\{ c/\sqrt{\varepsilon_1} \cos\left( \sin^{-1}\left( \sin\xi_0^{(2)} / \sqrt{\varepsilon_1} \right) \right) \right\}, \tag{30b}$$

where $m$ is a positive integer. Suppose that these multiple reflections from the top and bottom interfaces of the first layer can be subtracted from the ones coming from deeper layers. The first pulse observed after such subtraction is due to the third interface. This pulse is measured after a time

$$t_3 = 2d_0/(c/\cos\xi_0) + 2d_1/(c_1/\cos\xi_1) + 2d_2/(c_2/\cos\xi_2), \tag{31}$$

where $d_2$ is the thickness of the second layer. By a similar procedure, one can obtain the dielectric constant and the dielectric thickness of the second layer.

Along the same line, the combination of reflections $m$ and $n$ from the first and second layers can be determined and subtracted from later measurements at times

$$t_{mn}^{(1)} = 2d_0/\left\{c/\cos\xi_0^{(1)}\right\} + 2md_1/\left\{c/\sqrt{\varepsilon_1}\cos\left(\sin^{-1}\left(\sin\xi_0^{(1)}/\sqrt{\varepsilon_1}\right)\right)\right\} + 2nd_2/\left\{c/\sqrt{\varepsilon_2}\cos\left(\sin^{-1}\left(\sin\xi_0^{(1)}/\sqrt{\varepsilon_2}\right)\right)\right\} \tag{32a}$$

$$t_{mn}^{(2)} = 2d_0/\left\{c/\cos\xi_0^{(2)}\right\} + 2md_1/\left\{c/\sqrt{\varepsilon_1}\cos\left(\sin^{-1}\left(\sin\xi_0^{(2)}/\sqrt{\varepsilon_1}\right)\right)\right\} + 2nd_2/\left\{c/\sqrt{\varepsilon_2}\cos\left(\sin^{-1}\left(\sin\xi_0^{(2)}/\sqrt{\varepsilon_2}\right)\right)\right\} \tag{32b}$$

Here, $m$ and $n$ are positive integers and the second layer has thickness $d_2$ and dielectric constant $\varepsilon_2$. This procedure can be repeated until all reflections are subtracted. Degeneracies in times of reflection should, however, be taken into consideration. In order to do that, full wave analysis should be carried out to determine the relative amplitudes of the pulses reflected from the various interfaces. This is necessary in order to be able to separate the pulses reflected from different layers but arriving at the same time instants.

## 5. CONCLUSION

In this work, the reflection and transmission properties of X-waves obliquely incident on a planar air-dielectric interface have been investigated. The analysis is based on a general pulsed plane wave representation [cf. Eq. (6)] of X wave-type solutions. In this picture, the X-wave is composed of a set of pulsed plane waves specified by wave vectors forming a conical surface. The individual pulsed components are tilted at an angle $\xi$ relative to the axis of propagation of the X-wave. This

representation can be used within a ray-theoretic framework to deduce several useful attributes of the incident X-wave, e.g., the axial and lateral widths of the pulse. Furthermore, this framework provides an accurate explanation of the disintegration of the transmitted field for an obliquely incident X-wave. Unlike the incident and reflected fields, the pulsed components of the transmitted field do not have wave vectors lying on a circular cone. The transmitted rays form a convoluted conic surface and instead of meeting in a single apex, they end up on a line segment. The length of the line segment increases as the pulse travels deeper into the second medium, thus, causing the dispersion of the transmitted field. The line segment of the convoluted conic surface is pulled out away from the interface when the first medium is air $((c_1/c_2) > 1)$. In contrast, it is folded inwards when the first medium is the dielectric material $((c_1/c_2) < 1)$. In the latter case, the pulsed components incident at angles larger than $\sin^{-1}(c_1/c_2)$ follow lateral rays and the line segment stops at the interface. This ray-theoretic approach provides a clear mental picture of the disintegration process of the transmitted field. The transmitted pulse travels a specific distance away from the interface before it starts to disperse. This dispersion-free distance depends on the original axial width of the incident X-wave. Qualitatively, one can argue that as long as the length of the line segment given in Eq. (27) is smaller than the axial width of the incident pulse, the transmitted field suffers little dispersion. The dispersion becomes significant when the two lengths become comparable.

The ray-theoretic analysis introduced in this paper provides a clear mental picture of the behavior of an X-wave incident on a planar interface separating two media. Such analysis becomes more effective when reflections from multi-layered media are considered. We have outlined an inverse procedure from which the properties of the various layers (e.g., their thickness and relative permittivities) can be determined from the arrival times of reflections of two different X-waves. This procedure depends on the fact that the speeds of X-waves in the various layers depend on the apex angle $\xi$ of the incident field. Finally, we should point out that the analysis provided in this paper should be supplemented by an analytic method in order to calculate the amplitudes of the reflected and transmitted pulses. This is done in an accompanying article [23], where a spectral superposition is used to represent the various electromagnetic field components and the boundary conditions at the interface are used to deduce the amplitudes of the reflected and

transmitted fields. For computational purposes, the Fourier spectral representation is transformed to an azimuthal angular superposition akin to the one given in Eq. (11). This angular superposition is then used to study the properties of the reflected and transmitted fields and to determine the depths at which the transmitted fields start to disperse.

## REFERENCES


1. Brittingham, J. N., "Focus wave modes in homogeneous Maxwell equations: Transverse electric mode," *J. Appl. Phys.,* Vol. 54, 1179–1189, 1983.
2. Ziolkowski, R. W., "Exact solutions of the wave equation with complex source locations," *J. Math. Phys.,* Vol. 26, 861–863, 1985.
3. Sezigner, A., "A general formulation of focus wave modes," *J. Appl. Phys.,* 57, 678, 1985.
4. Ziolkowski, R. W., "Localized wave physics and engineering," *Phys. Rev. A,* Vol. 44, 3960–3984, 1991.
5. Wu, T. T., "Electromagnetic missiles," *J. Appl. Phys.,* Vol. 57, 2370–2373, 1985.
6. Shen, H. M., and T. T. Wu, "The properties of the electromagnetic missile," *J. Appl. Phys.,* Vol. 66, 4025–4034, 1989.
7. Heyman, E., and L. B. Felsen, "Propagating pulsed beam solutions by complex parameter substitution," *IEEE Trans. Antennas Propagat.,* Vol. 34, 1062–1065, 1986.
8. Heyman, E., B. Z. Steinberg, and R. Ianconescu, "Electromagnetic complex source pulsed beam fields," *IEEE Trans. Antennas and Propagat.,* Vol. 38, 957–963, 1990.
9. Saari, P., and K. Reivelt, "Evidence of X-shaped propagation-invariant localized light waves," *Phys. Rev. Lett.,* Vol. 21, 4135–4138, 1997.
10. Saari, P., and H. Sõnajalg, "Pulsed Bessel Beams," *Laser Phys.,* Vol. 7, 32–39, 1997.
11. Lu, J. Y., and J. F. Greenleaf, "Experimental verification of nondiffracting X waves," *IEEE Trans. Ultrason. Ferroelec. Freq. Contr.,* Vol. 39, 441–446, 1992.
12. Lu, J. Y., and J. F. Greenleaf, "Nondiffracting X waves — exact solutions to free space scalar wave equation and their finite aperture realization," *IEEE Trans. Ultrason. Ferroelec. Freq. Contr.,* Vol. 39, 19–31, 1992.
13. Daniels, D. J., *Surface-Penetrating Radar,* IEE Press, 1996.
14. Taylor, J. D. (Ed.), *Introduction to Ultra-Wideband Radar Systems,* CRC Press, 1995.

15. Besieris, I. M., M. Abdel-Rahman, A. Shaarawi, and A. Chatzipetros, "Two fundamental representations of localized pulse solutions of the scalar wave equation," *Progress in Electromagnetics Research (PIER),* Vol. 19, 1–48, 1998.
16. Shaarawi, A. M., "Comparison of two localized wavefields generated from dynamic apertures," *J. Opt. Soc. Am. A,* Vol. 14, 1804–1816, 1997.
17. Shaarawi, A. M., S. M. Sedky, F. M. Taiel, R. W. Ziolkowski, and I. M. Besieris, "Spectral analysis of time-limited pulsed Gaussian wavefields," *J. Opt. Soc. Am. A,* Vol. 13, 1817–1835, 1996.
18. Fagerholm, J., A. T. Friberg, J. Huttunen, D. P. Morgan, and M. M. Salomaa, "Angular-spectrum representation of nondiffracting X waves," *Phys. Rev. E,* Vol. 54, 4347–4352, 1996.
19. Friberg, A. T., J. Fagerholm, and M. M. Salomaa, "Space-frequency analysis of nondiffracting pulses," *Opt. Comm.,* Vol. 136, 207–212, 1997.
20. Shaarawi, A. M., R. W. Ziolkowski, and I. M. Besieris, "On the evanescent fields and the causality of the focus wave modes," *J. Math. Phys.,* Vol. 36, 5565–5587, 1995.
21. Hillion, P., "How do focus wave modes propagate across a discontinuity in a medium?" *Optik,* Vol. 93, 67–72, 1993.
22. Donnelly, R., and D. Power, "The behavior of electromagnetic localized waves at a planar interface," *IEEE Trans. Antennas Propagat.,* Vol. 45, 580–591, 1997.
23. Shaarawi, A. M., I. M. Besieris, A. M. Attiya, and E. A. El-Diwany, "Reflection and transmission of an electromagnetic X-wave incident on a planar air-dielectric interface: spectral analysis," submitted to *J. Electromagn., Waves Appl.*.
24. Shaarawi, A. M., I. M. Besieris, A. M. Attiya, and E. El-Diwany, "Acoustic X-wave reflection and transmission at a planar interface: spectral analysis," *J. Acoust. Soc. Am.,* Vol. 107, 70–86, 2000.
25. Gradshteyn, I. S., and I. M. Ryzhik, *Tables of Integrals, Series and Products,* Academic Press, NY, 1965.
26. Chatzipetros, A. A., A. M. Shaarawi, I. M. Besieris, and M. A. Abdel-Rahman, "Aperture synthesis of time-limited X-waves and analysis of their propagation characteristics," *J. Acoust. Soc. Am.,* Vol. 103, 2287–2295, 1998.